

A Method for Constraining Cosmic Magnetic Field Models Using Ultra-High Energy Cosmic Rays: The Field Scan Method

Michael S. Sutherland*

*Department of Physics and Astronomy,
Louisiana State University, Baton Rouge, LA 70803, USA*

Brian M. Baughman[†]

Department of Physics, University of Maryland, College Park, MD 20742, USA [‡]

J. J. Beatty[§]

*Department of Physics and the Center for Cosmology and Astro-Particle Physics,
The Ohio State University, Columbus, Ohio 43210, USA*

Abstract

The Galactic magnetic field, locally observed to be on the order of a few μG , is sufficiently strong to induce deflections in the arrival directions of ultra-high energy cosmic rays. We present a method that establishes measures of self-consistency for hypothesis sets comprised of cosmic magnetic field models and ultra-high energy cosmic ray composition and source distributions. The method uses two independent procedures to compare the backtracked velocity vectors outside the magnetic field model to the distribution of backtracked velocity directions of many isotropic observations with the same primary energies. This allows for an estimate of the statistical consistency between the observed data and simulated isotropic observations. Inconsistency with the isotropic expectation of source correlation in both procedures is interpreted as the hypothesis set providing a self-consistent description of GMF and UHECR properties for the cosmic ray observations.

INTRODUCTION

Ultra-high energy cosmic rays (UHECRs) are almost certainly extragalactic in origin as no anisotropy is observed except at the highest energies [1]. UHECRs are also thought to be largely comprised of charged particles [2] and will therefore experience magnetic deflection during propagation from their sources. This deflection can be sufficiently large as to make source identification difficult.

The UHECR magnetic deflection is thought to arise as two distinct contributions: extragalactic and Galactic. Turbulent magnetic fields are expected to comprise the dominant component in extragalactic space with nG field strength upper limits [3–7]. There is disagreement regarding the expected typical deflection, ranging from less than a few degrees to tens of degrees (see, e.g., [8–13]). However, these studies are highly sensitive to simulation conditions, such as propagation through filaments and voids with strong and weak fields, respectively.

The deflection induced by the Galactic magnetic field (GMF) is thought to dominate over the extragalactic deflection (see, e.g., [13–20]), owing to the significantly larger field strengths and more organized (regular) field structure. Simulated isotropically observed cosmic rays are backtracked through particular GMF configurations to determine the typical deflection magnitudes along different sight-lines. Deflection magnitudes at least of order few degrees are common, even for proton primaries with energies greater than a few 10^{18} eV.

However, the GMF structure is not well-known aside from the neighborhood of the Sun. Near the Sun, the local field is observed to point towards Galactic longitude $\ell \approx 80^\circ$ in the Galactic plane [21–23] following the stellar spiral arm with a regular component field strength of order few μG [24–28]. The turbulent component is thought to be of roughly the same magnitude with typical cell sizes less than 100 pc [26, 29–32]. Larger field strengths are observed closer to and within the Galactic center (see, e.g., [33]). A regular component extends to a distance of at least 500 pc from Galactic plane (see, e.g., [34]). Galactic halo fields may extend well beyond this according to expectations with the Galactic electron distribution (see, e.g., [35]). There is additionally disagreement regarding the number and location of field reversals within the disk, although there is strong evidence of at least one reversal inside the solar circle and possibly none outside (see, e.g., [24, 27, 36, 37]).

There is currently no consensus on the structure of the large-scale regular component

of the GMF [26, 38, 39]. Observations of magnetic fields in similar galaxies may provide clues regarding the magnetic structure of the Galaxy. Spiral galaxies are typically observed to possess a regular magnetic field component following the spiral arms [3, 5, 40]. In the interarm regions, the regular magnetic field dominates over the turbulent component, and vice-versa within the arms [41–44]. Observed field strength magnitudes are typically of order $1 - 25 \mu\text{G}$ within the disk [5, 26, 40]. However, numerous starburst galaxies have been observed with magnetic field strengths of up to $100\mu\text{G}$ [45–48].

Assuming an extragalactic source distribution, one could backtrack observed cosmic rays through various field models until a significant number coincided with hypothesized sources. However, a large number of coincident events may simply be a feature of a field model despite knowing the UHECR composition and source distribution. Harari et al. [17] have shown that certain GMF models exhibit lensing that focuses cosmic ray trajectories onto specific parts of the extragalactic sky. This effect may artificially increase the number of coincident correlations with hypothesized sources located in regions where lensing is strong. For example, the report [49] of a strong correlation between the backtracked AGASA UHECR dataset and selected BL Lac objects was found to be highly dependent on the composition and GMF hypotheses [19].

In this paper a method for determining self-consistency of cosmic magnetic field model and cosmic ray property hypothesis sets for UHECR datasets is presented, henceforth referred to as the Field Scan Method (FSM). The cosmic ray dataset and many isotropic simulations are backtracked to determine the extragalactic arrival distribution. An isotropic arrival distribution of cosmic rays at Earth will propagate back through the magnetic field and map into a non-isotropic extragalactic arrival distribution due to magnetic lensing. A highly anisotropic sky distribution and an excess of coincident events with the hypothesized source distribution compared to the expectation derived from the isotropic simulations serve as indications that the magnetic field model together with the composition and source distribution hypotheses provide a self-consistent description of the cosmic ray observations. The comparisons against isotropy allow for the hypothesis consistency test even in a scenario where magnetic lensing is strong along particular lines of sight. Preliminary implementations of this method were explored in [50, 51], however, in this paper we optimize the analysis with respect to the previously applied methods. Table I contains a reference list of acronyms used throughout the text.

TABLE I: Table of Acronyms

DOI	Dataset of interest
MCISOs	Monte Carlo simulations of isotropy
$N_{corr}^{DOI}, \bar{N}_{corr}^{iso}$	Number of correlating events in the dataset
\bar{N}_{corr}^{iso}	Mean number of correlating events in the isotropic simulations
P_{bin}	Probability of drawing N_{corr}^{DOI} correlating events from a binomial distribution defined by the correlation properties of the isotropic simulations
D_{max}, P_{KS}	Maximum signed difference between the dataset and isotropic test statistic distributions and the probability that the distributions result from the same parent distribution
Θ_{sep}^{min}	Normalized minimum angular separation between the magnetically-corrected arrival direction and the assigned “nearest” source object
δ_B	Angular deflection magnitude of an event
Ψ	Test statistic
θ_{src}	Actual angular distance between an event and a source object
δ_{turb}	RMS angular deflection from a turbulent magnetic field
RADIO	Catalog of radio galaxies
RADIO+SWIFT39	Catalog of radio galaxies and selected objects in the Swift 39-month catalog
ISOTROPIC80	List of 80 isotropically selected directions
VCV	12 th Edition Véron-Cetty and Véron catalog
BSS_A, ASS_S	Two variation of logarithmic sprial GMF models

PROCEDURE

The FSM provides an estimate of hypothesis set self-consistency by comparing the behavior of an UHECR dataset of interest (DOI) folded with the hypothesis set against that of Monte Carlo simulations of isotropy (MCISOs). Figure 1 shows the general procedure of the method. Hypothesis sets contain three independent components: observed composition,

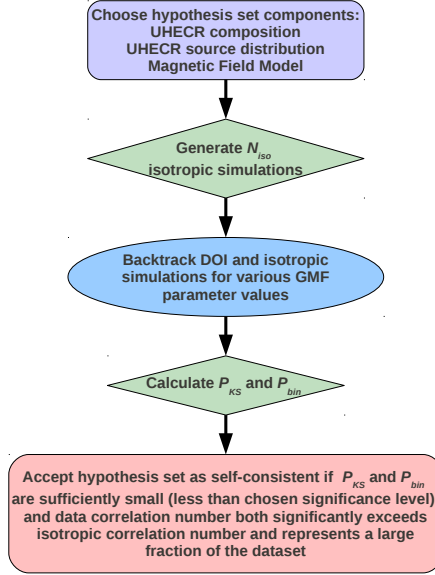


FIG. 1: Methodology of the Field Scan Method.

source distribution¹, and a magnetic field configuration. The MCISOs are constructed with the same DOI energies, but with directions sampled from a homogeneous isotropic flux, in the vicinity of where the observations were taken, modulated by detector coverage matching that of the DOI. The method is strongly dependent on the underlying hypothesis set components. The correctness of individual hypothesis components cannot be determined, only that the set is self-consistent in its entirety.

The essential idea behind the method is to find regions of the hypothesis set parameter space² for which source correlation and consistency with the isotropic simulations are maximized and minimized respectively. Such regions of parameter space cannot be ruled out as self-consistent theories describing the observed composition, source distribution, and magnetic field, therefore meriting further examination. Regions of parameter space where the DOI is found to be more consistent with the MCISOs or exhibit unidentifiably significant source correlation represent hypotheses which are not self-consistent and can thus be ruled out as viable theories.

Self-consistency is determined by two independent procedures: (1) correlation using angular windows and (2) a statistical test performed on the distribution of an event-by-event

¹ Any catalog which correlates well with the true source distribution will show a deviation from the correlation expectation from isotropy.

² That is, any parameters which are not otherwise constrained.

test statistic (TS) for the DOI and MCISOs. In procedure (1), a correlation number is determined by counting the events which fall within a specified angular window around the source objects after magnetic correction. The DOI correlation number is then compared to the correlation number distribution from the isotropic simulations. For small angular windows the isotropic correlation number distribution closely matches a binomial distribution, so that the binomial probability P_{bin} of obtaining the DOI correlation value can be computed from,

$$P_{bin}(k; n, p) = \binom{n}{k} p^k (1 - p)^{n-k} \quad (1)$$

The probability of success p can be approximated by $(\overline{N}_{corr}^{iso} / N_{tot})$, where $\overline{N}_{corr}^{iso}$ is the mean number of correlating events from many isotropic instances and N_{tot} is the total number of events in the DOI or a single isotropic instance. P_{bin} can be calculated using $k = N_{corr}^{DOI}$ and $n = N_{tot}$. A large positive excess of correlating events will yield a small probability, indicating that the hypothesis set is self-consistent. A negative or small positive excess indicates that the DOI does not correlate more than the isotropic expectation and does not indicate identifiable self-consistency. Magnetic lensing onto a portion of the sky containing many source objects may present a scenario where N_{corr}^{DOI} itself is large but the excess small.

Procedure (2) is designed to identify those hypothesis sets that do not produce identifiably significant source correlation. It determines the compatibility between distributions of event-by-event TS values for the DOI and MCISOs. After backtracking the i^{th} event using the hypothesized composition and magnetic field model the test statistic,

$$\Psi_i = \frac{\Theta_{sep,i}^{min}}{1. + \delta_{B,i}} \quad (2)$$

is calculated where i denotes the i^{th} event, $\delta_{B,i}$ is the angular deflection magnitude between the observed and magnetically-corrected arrival vectors, and $\Theta_{sep,i}^{min}$ is the normalized minimum angular separation between the magnetically-corrected arrival vector and the assigned “nearest” source object. This construction of Ψ_i does not diverge as the magnitude of the magnetic field goes to zero ($\delta_{B,i} \rightarrow 0$) and is minimized when $\Theta_{sep,i}^{min}$ is also minimized (for monotonic $\delta_{B,i}$). A normalized minimum angular separation can incorporate an estimate of deflection through a turbulent magnetic field, e.g., an extragalactic magnetic field. Such fields have been shown to induce a gaussian smearing effect on the velocity vectors of UHE-CRs injected into them [52]. For example, the assigned “nearest” source object could be

that which minimizes the ratio $\theta_{src}/\delta_{turb}$, where θ_{src} is the actual angular distance between the backtracked event and a source object and δ_{turb} is the estimate of RMS magnetic deflection from the source object induced by a fixed parameter turbulent field. The RMS deflection magnitude would depend on the characteristic magnitude and correlation length of the turbulent model, as well as the event energy and source distance. In such a case $\Theta_{sep}^{min} = \min(\theta_{src}/\delta_{turb})$. In cases where no such turbulent field is modeled, Θ_{sep}^{min} would be simply $\min(\theta_{src})$. Use of a normalized minimum angular separation in general can allow for the use of a much deeper, in redshift, catalog as this normalization scales the correlation window with distance from the source.

The statistical compatibility of the full DOI with the MCISOs is determined using a Kolmogorov-Smirnov (KS) test³ between the distributions of Ψ_i^{DOI} for the DOI and Ψ_j^{MCISO} for MCISOs. This test employs the cumulative distribution function (CDF) of Ψ_i distribution and determines the maximum signed difference D_{max} of the quantity,

$$D_i = CDF^{DOI}(\Psi_i) - CDF^{MCISO}(\Psi_i) \quad (3)$$

between the Ψ_i CDFs of the DOI and MCISO. D_{max} maps to the probability P_{KS} that the distribution from which the Ψ_i^{DOI} values are drawn is similar to the distribution from which the Ψ_j^{MCISO} values are drawn. As constructed in Eqn. 2, a smaller Ψ_i indicates stronger correlation between the hypothesized source distribution and the backtracked trajectory of the tested event. By examining the sign and location of D_{max} , it is possible to determine if source correlations are increasing under the hypothesis set. This ensures that the entire hypothesis set (composition, magnetic field model, and source distribution) is being tested and that the minimum in consistency between Ψ_i^{DOI} and Ψ_j^{MCISO} is indicating an increased correlation with the source distribution.

The hypothesis set is deemed self-consistent to the extent that the P_{KS} value indicates inconsistency with isotropy and that the DOI correlates well with the source hypothesis. A large positive D_{max} , resulting in small P_{KS} , located at a small TS value indicates that the DOI better correlates with the source hypothesis than the isotropic expectation and is inconsistent with the isotropic expectation. Conversely, if the dataset differs little from the isotropic expectation (small D_{max} and large P_{KS}), then one or more of the hypothesis components may be incorrect, or perhaps the method is probing a regime where self-consistency

³ Other hypothesis testing algorithms can be easily substituted.

cannot be identified (e.g., strong lensing that hinders identification of significant source correlation beyond the isotropic expectation). Positive D_{max} at large TS values and any negative D_{max} are also indicators of these scenarios.

A typical significance level for rejecting the null hypothesis (the DOI and isotropic TS distributions appear to be drawn from the same parent distribution) is $\alpha = 1\%$, i.e., $P_{KS} < 0.01$. This value is appropriate for determining whether the DOI is similar to isotropy in this method.

These procedures provide complementary results. Procedure (1) allows for a numerical correlation estimate as well as the probability of such result, but is insensitive to details of the backtracked sky distribution and the final locations of the events around the source objects. Procedure (2) incorporates the source separation and magnetic deflection magnitude for every event to determine the overall consistency between the backtracked sky distributions for the DOI and MCISOs. Significant deviations from the expectation of isotropic correlation are expected in both procedures under a hypothesis set that correctly describes the UHECR observations.

VALIDATION

The FSM has been tested by simulating a variety of simple truth scenarios, as well as spanning more realistic configurations of magnetic fields and UHECR composition and source distributions. Here we present the results of one such simple scenario; realistic scenarios are briefly described at the end of this section.

A mock universe is constructed using the parameters of Table II. 20 cosmic ray events were generated such that, when backtracked through the truth magnetic field model configuration assuming the truth composition, they lie within 0.01° of an object from the truth source distribution. The true source positions and the observed arrival directions are shown in Figure 2. The truth hypothesis set is tested to confirm that both methods correctly identify self-consistency at the correct field parameter values and that self-consistency decreases as the hypothesis set is altered. Various non-truth hypothesis sets are also tested to determine the possibility of generating a false signal. These simulations are backtracked using *CRT*, a public numerical tool for propagating UHECRs through magnetic field model models [53].

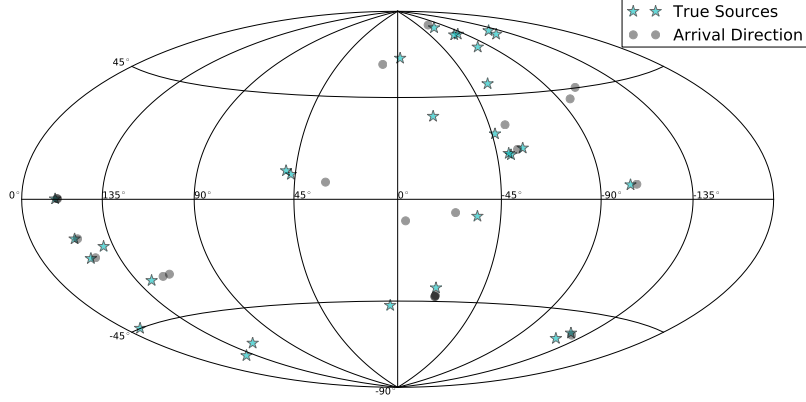


FIG. 2: Observed arrival directions (shaded black circles) and positions of their true sources (blue stars) of the 20 cosmic rays in the validation scenario.

TABLE II: Truth Scenario

Composition	Pure proton
Source Distribution	RADIO
GMF	Pure Dipole
Local Field Strength (B_{\odot})	$1.5 \mu\text{G}$

Composition Hypothesis Component

A pure proton composition is hypothesized for all combinations of source and GMF hypothesis components.

GMF model component

The parameter space of two distinct models are scanned: pure dipole and pure uniform. The pure dipole is the truth field. In both models, the only parameter is the local field strength which is scanned from $-1.0 \mu\text{G}$ to $3.0 \mu\text{G}$ in steps of $0.1 \mu\text{G}$. A positive dipole field strength gives a field vector oriented towards the North Galactic Pole. The uniform

field is oriented towards the Galactic longitude $\ell = 90^\circ$ for positive field magnitudes, i.e. perpendicular to the direction of the Galactic center and wholly parallel to the Galactic plane. Galactic turbulent fields are not modeled nor any turbulence in extragalactic space. Both fields have zero magnitude beyond a galactocentric distance of 20 kpc.

Source Catalogs

Three individual source distributions are tested: a selection of 29 radio galaxies [54] (RADIO) which also comprise the truth source distribution, a combination of RADIO and the Palermo Swift-BAT hard X-ray catalog [55] (RADIO+SWIFT39), and a catalog comprised of 80 isotropically selected directions (ISOTROPIC80). A redshift cut of $z_{max} \leq 0.018$ is applied only to RADIO+SWIFT39 resulting in 127 objects (21 from RADIO and 106 from SWIFT39).

Results

We first perform a scan over the truth hypothesis set (Proton, RADIO, Dipole) at $B_\odot = 1.5 \mu\text{G}$ by varying the number of isotropic instances N_{iso} used to determine P_{KS} . This will allow a determination of an appropriate N_{iso} that balances accurate modeling of isotropy with computation time. 100 unique simulations are generated for each value of N_{iso} in the range $(10^2, 10^{2.5}, \dots, 10^5)$. The resulting distributions of P_{KS} are shown in Figure 3. For large values of N_{iso} , the mean of the distribution approaches a constant value and the distribution itself tightens, as illustrated by the red error bars. There appears to be no gain in accuracy or precision beyond $N_{iso} = 10^4$ and only corresponding increases in computation time.

We now scan the magnetic field strength parameter space of the truth hypothesis set between -1.5 and $3.0 \mu\text{G}$. At each field strength point, we generate 100 simulations each comprised of $N_{iso} = 10^4$ unique isotropic instances. Figure 4a indicates that the mean isotropic correlation number is essentially constant across all scanned field strengths, whereas better correlation in the DOI is observed closer to the correct magnetic field arrangement. A very clear minimum in P_{KS} is also observed in coincidence with the highest source correlation at the correct field strength value in Figure 4b.

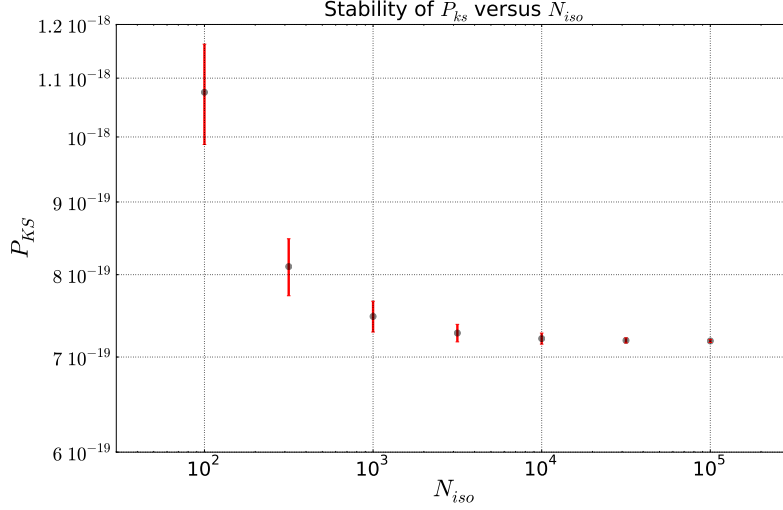


FIG. 3: Distribution of P_{KS} for 100 simulations at different values of N_{iso} . The red error bars depict the spread of the distribution at each point.

Figure 5 shows a histogram of the correlation number for various angular windows for 10^4 isotropic instances at $B_\odot = 1.5 \mu\text{G}$. The error bars are calculated using Poisson statistics on each histogram bin entry. The circles depict binomial distributions calculated according to $p = \bar{N}_{corr}^{iso} / N_{tot}$ as described previously and are color-coded to their respective histograms. KS tests performed between each N_{corr}^{iso} distribution and its derived binomial distribution show clear agreement. For small angular windows the isotropic correlation number distribution is well-described by a binomial distribution. The binomial distribution approximation for small angular windows remains applicable even for parameter values and hypothesis sets distinct from truth.

Figure 6 shows P_{bin} calculated from N_{corr}^{DOI} according to Eq. 1. The minimum P_{bin} occurs at $B_\odot = 1.4 \mu\text{G}$ due to statistical variation in the \bar{N}_{corr}^{iso} , however, the strongest correlation (all 20 events) is correctly observed in the adjacent field strength bin. It is clear from these figures that both methods correctly identify the magnetic field parameters of the truth hypothesis set and that the hypothesis set is most self-consistent at those values. As the field strength is detuned from the truth value the hypothesis set does not allow for complete correlation and becomes a self-inconsistent description of the cosmic ray observations.

We note that such extreme values of P_{KS} and P_{bin} arise from the contrived nature of the scenario. Any realistic application of this method to real cosmic ray observations would lead to much larger values and smaller variations of these probability measures in accordance

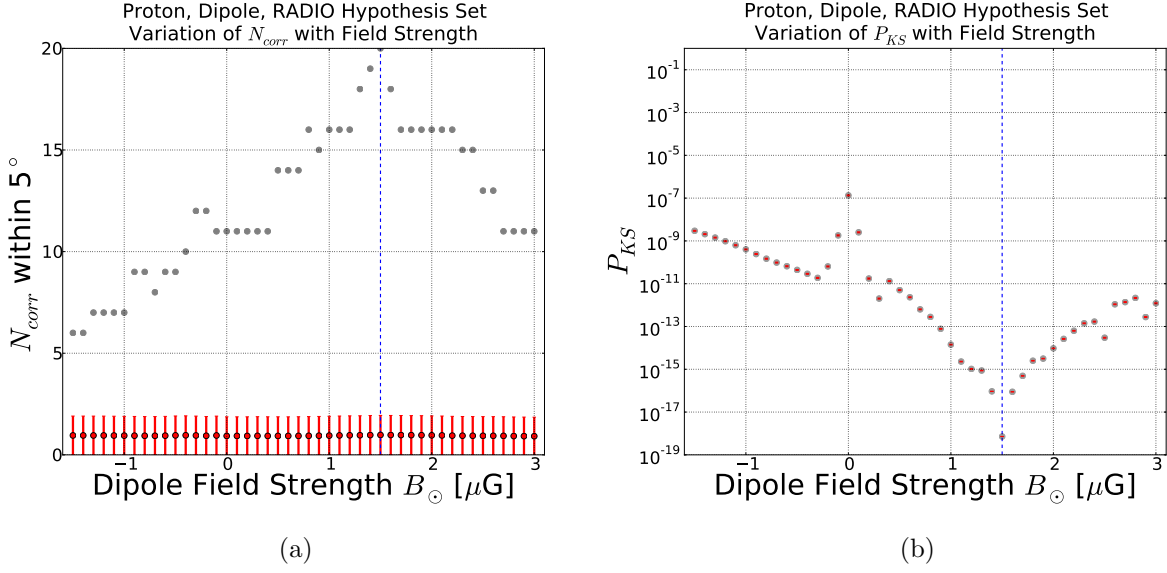


FIG. 4: Magnetic field strength scan of the truth scenario. The truth field strength is indicated by the dashed blue line. The left plot shows the number of events correlating with RADIO sources within 5° windows. The red dots and error bars indicate the mean and spread of the isotropic correlation number distributions. The right plot shows the distribution of P_{KS} . The red shaded dots and red lines indicate the mean and spread of the P_{KS} distribution from the 100 isotropic simulations.

with the greater level of uncertainty in real datasets and knowledge of their environment.

We now begin to vary the components of the hypothesis sets. Figures 7 and 8 show the variation of P_{KS} and P_{bin} for hypothesis sets incorporating RADIO+SWIFT39 and ISOTROPIC80 with a proton composition and the dipole model. Due to the fact that some of the true sources are a subset of the RADIO+SWIFT39, P_{KS} is minimized at a comparable value to that in Figure 4b since the Ψ_i^{DOI} distribution is unchanged. The DOI events are not distributed similarly to isotropy after being backtracked. However, Figure 8a shows that source correlation is more consistent with the mean isotropic expectation. At $B_\odot = 1.5 \mu\text{G}$, $N_{corr}^{DOI} = 20$ but the larger number of source objects in this catalog increases the number of random correlations so that P_{bin} is increased to 10^{-5} . Although such a large deviation from isotropy and high value of N_{corr}^{DOI} could prompt further investigation, these results do not indicate a self-consistent description of the hypothesis set.

The hypothesis set incorporating the ISOTROPIC80 source distribution is also observed

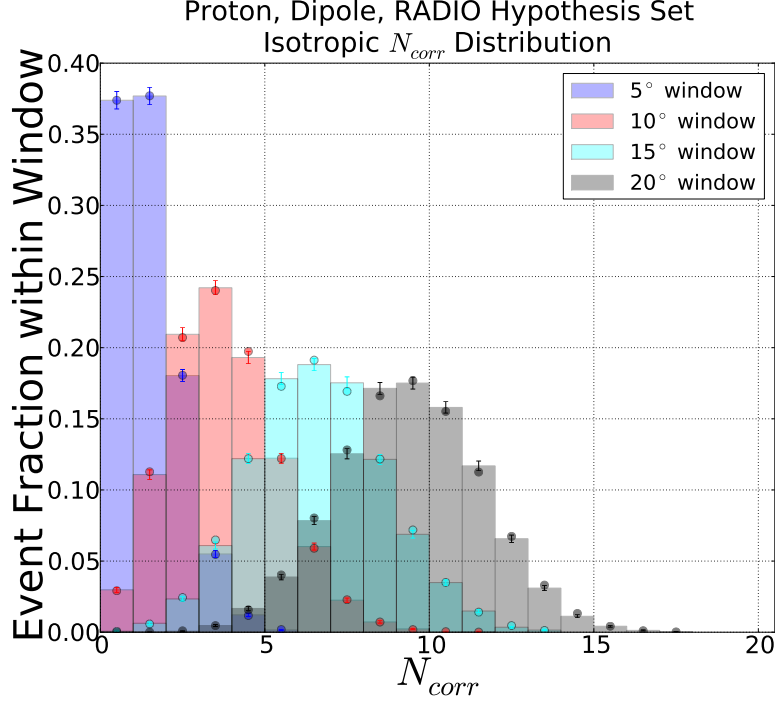


FIG. 5: Histogram of N_{corr} for different angular windows for 10^4 isotropic instances at $B_{\odot} = 1.5 \mu\text{G}$. The error bars are Poisson error statistics on each histogram bin entry. The dots show the probability values for a binomial distribution derived from the mean correlation fraction of each angular window histogram.

to not be self-consistent in Figures 7b and 8b. The Ψ_i^{DOI} distribution is consistent with the isotropic expectation. Although it begins to decrease at larger field strength it still lies at large values ($P_{KS} > 10^{-2}$). However, no correlation excess is observed in concert with a smaller P_{KS} . This indicates that the backtracked DOI is not behaving in a manner similar to isotropy, but it is not correlating with the hypothesized source distribution, therefore ruling this hypothesis set self-inconsistent.

Figures 9 and 10 show the variation of P_{KS} and N_{corr} versus the field strength for hypothesis sets incorporating the uniform field model. These 3 hypothesis sets do not increase source correlations and are not self-consistent descriptions. Indeed for the RADIO source hypothesis in Figure 10a, while the “observed” ($B_{\odot} = 0 \mu\text{G}$) P_{bin} is small, the presence of a nonzero field serves only to lower the correlation count which contradicts the explicit assumption that the hypothesis set is correct.

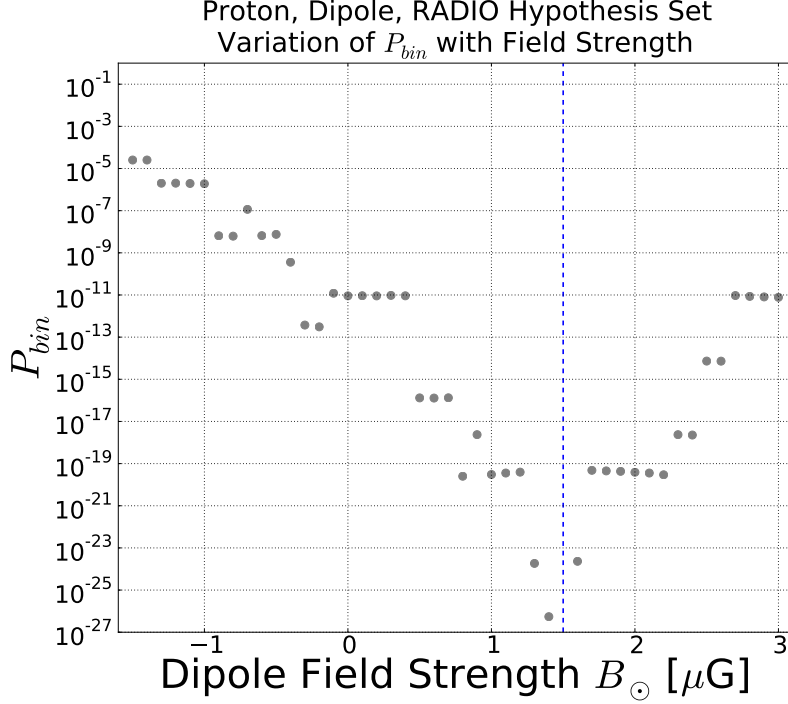


FIG. 6: Field scan of the truth scenario. The truth parameter point is at $B_{\odot} = 1.5 \mu\text{G}$ as indicated by the dashed blue line.

Additional Scenarios

In addition to the simple scenario described previously, we have also investigated situations where the truth DOI UHECR properties and GMF are more consistent with observations and theoretical expectations proposed in the literature [14, 16, 39, 56]. The truth of two such scenarios are detailed in Table III. The VCV catalog listed in the table is the 12th Edition Véron-Cetty and Véron catalog of quasars and active nuclei [57]. The BSS_A and ASS_S field types are logarithmic spiral GMF models [16]. These scenarios are representative of the results found during the extensive validation process.

To make the validation more realistic the fraction of source to isotropic (background) events has also been varied⁴. The arrival directions of the mock events incorporate observational resolution⁵ and the sky coverage matches that of the southern site of the Pierre Auger Observatory, as shown in Figure 11. During the hypothesis set scanning procedure, additional deflection due to an extragalactic turbulent magnetic field is applied to the

⁴ Any set of UHECR observations will contain events which come from sources not in a catalog and not directly from the source, e.g. GZK daughter particles.

⁵ These scenarios use the detector resolution of the Pierre Auger Observatory [58].

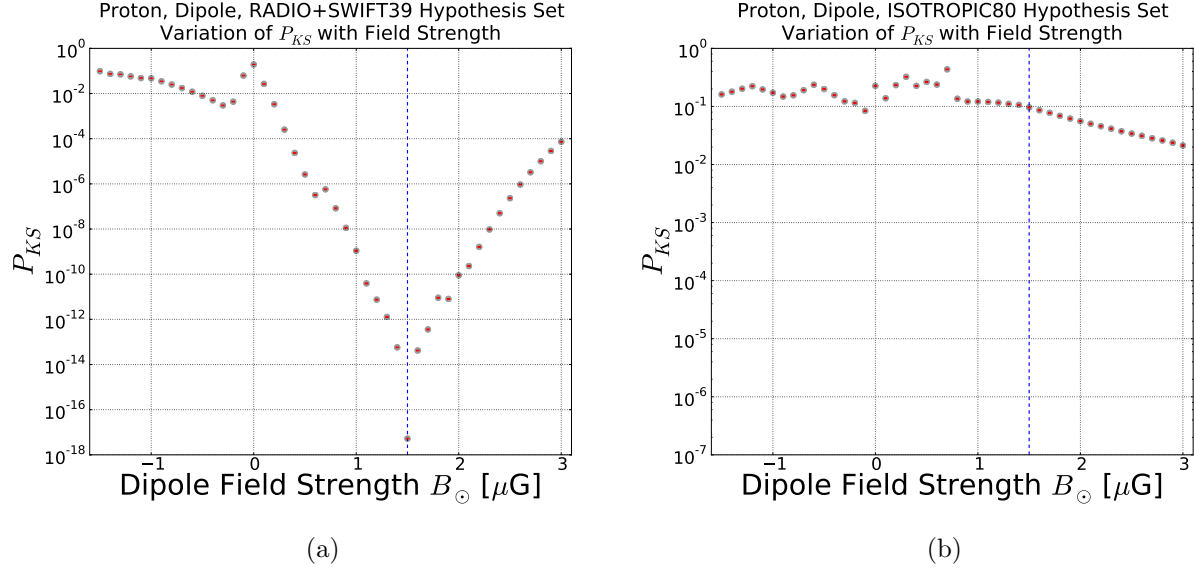


FIG. 7: Variation of hypothesis set components. The field is the dipole model and the truth parameter point is at $B_{\odot} = 1.5 \mu\text{G}$ as indicated by the dashed blue lines. The source components are RADIO+SWIFT39 (left), and ISOTROPIC80 (right). The shaded dots and red lines indicate the mean and spread of the P_{KS} distribution from the 100 isotropic simulations.

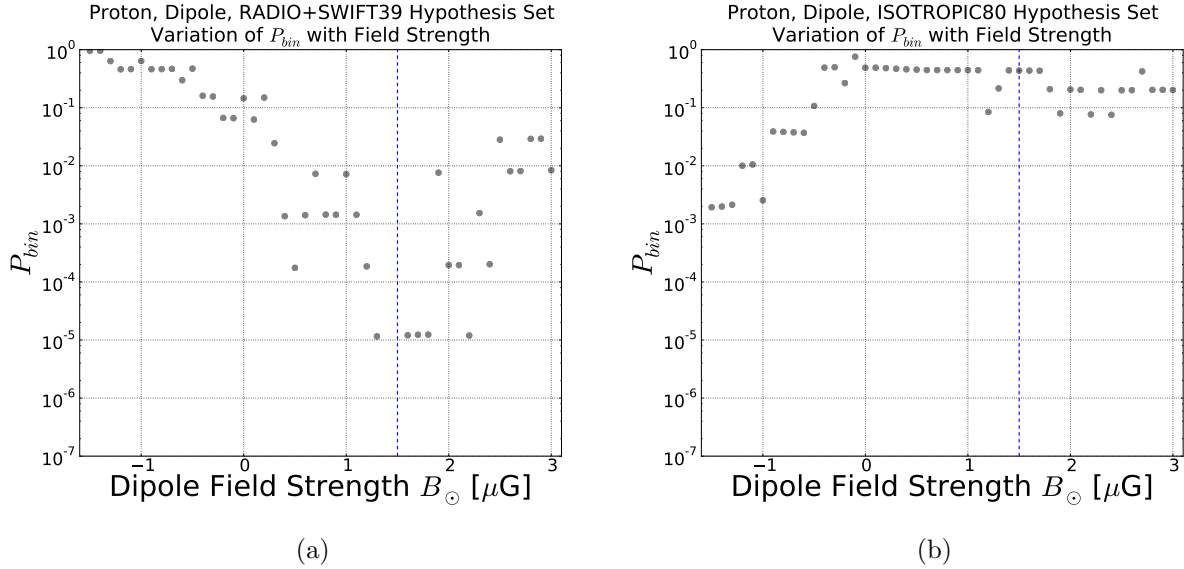


FIG. 8: Variation of hypothesis set components. The field is the dipole model and the truth parameter point is at $B_{\odot} = 1.5 \mu\text{G}$ as indicated by the dashed blue lines. The source components are RADIO+SWIFT39 (left), and ISOTROPIC80 (right).

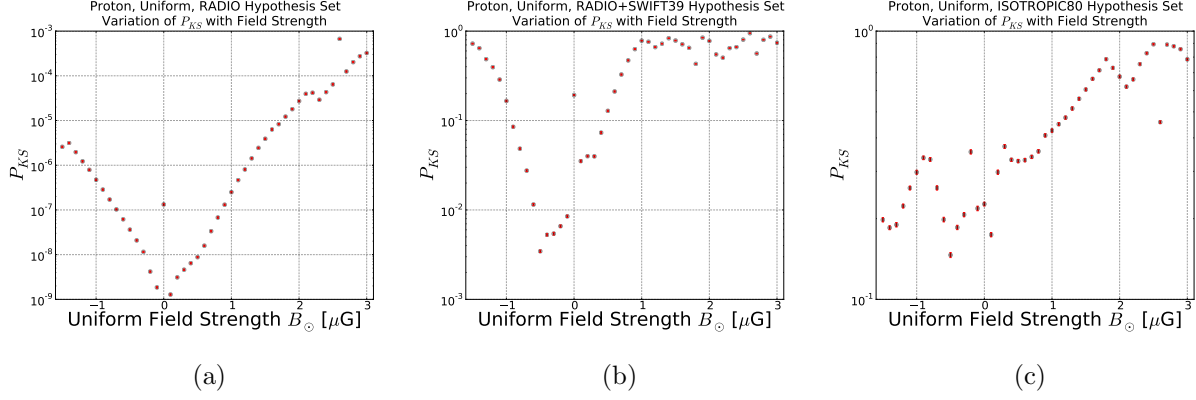


FIG. 9: Variation of hypothesis set components. The field is the uniform model. The source components are RADIO (left), RADIO+SWIFT39 (middle), and ISOTROPIC80 (right). The shaded dots and red lines indicate the mean and spread of the P_{KS} distribution from the 100 isotropic simulations.

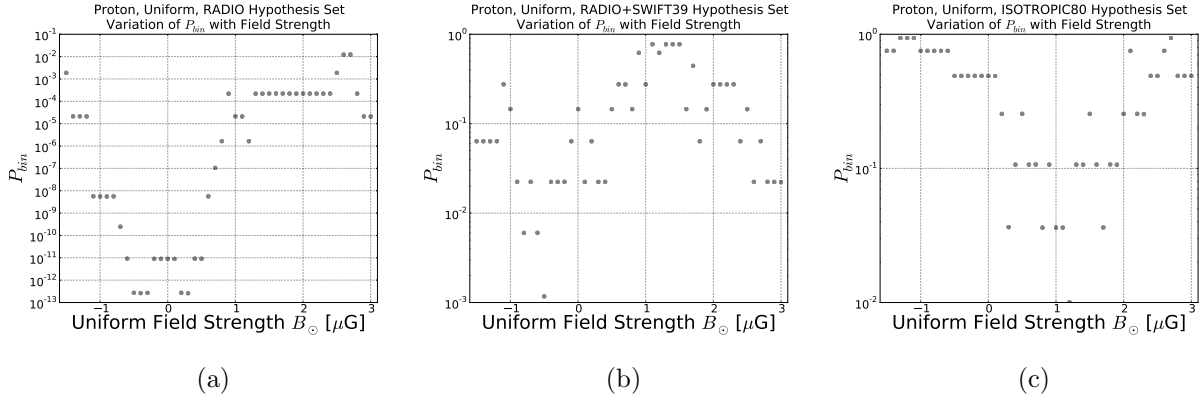


FIG. 10: Variation of hypothesis set components. The field is the uniform model. The source components are RADIO (left), RADIO+SWIFT39 (middle), and ISOTROPIC80 (right).

post-backtracked arrival direction by sampling a gaussian smear function centered on the backtracked direction; propagation through extragalactic space is not performed by *CRT*.

The method behaves as expected near the truth values and does not produce false positives for all realistic validation scenarios. Proton truth scenarios continue to show a dramatic decrease in the consistency between the DOI and the MCISOs, which is maximal in the magnetic field parameter space immediately surrounding the truth value. Furthermore, as the field strength is increased the consistency decreases towards the truth value. That is, as

TABLE III: Truth Scenarios

	I	II
Composition	Pure proton	Pure Iron
Isotropic Fraction	50%	0%
Source Distribution	VCV Catalog ($z \leq 0.017$)	Swift 39 Month Catalog ($z \leq 0.021$)
Field Type	BSS_A	ASS_S
Local Field Strength (B_\odot)	$0.71 \mu\text{G}$	$1.9 \mu\text{G}$
Planar Scale Height (z_1)	0.95 kpc	1.2 kpc
Field Pitch Angle (p)	-9.6°	-13.1°

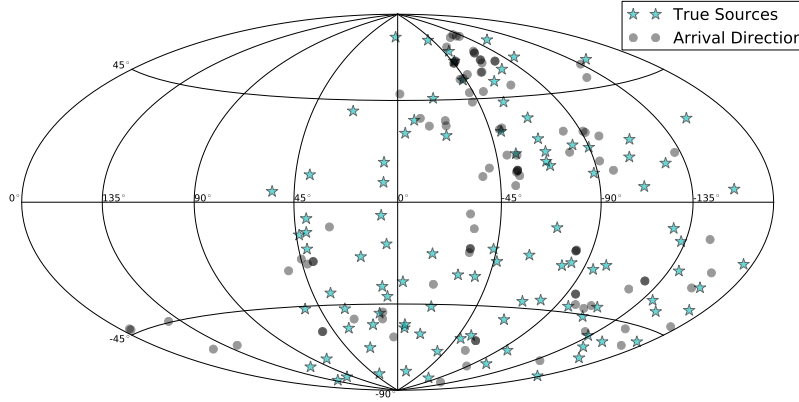


FIG. 11: Observed arrival directions (shaded black circles) and positions of their true sources (blue stars) of the events in the realistic Truth Scenario I.

the field turns on, correlations with the source distribution increase more than would be expected from an isotropic sample. Figure 12 shows contour plots for various hypothesis sets for the Truth Scenario I as functions of the local field strength and orientation. The value of P_{KS} at each point is smeared using a two dimensional gaussian kernel to minimize the effects of limited statistical samples. The un-smeared surfaces do not show any important features not displayed in the smeared figures. The truth realization is indicated as a star in the

corresponding parameter space subplot. Clear deviation from the isotropic expectation is observed; maximal deviation from isotropy occurs at the same parameter point as maximal source correlation for the truth hypothesis set.

The presence of a turbulent Galactic magnetic field component in addition to the regular component may have a significant effect on the identification of hypothesis set self-consistency. In a separate study [51] it was found that magnetic turbulence typically isotropizes cosmic rays. Compared to the P_{KS} value for a GMF with no turbulence, P_{KS} for a turbulent GMF is typically larger. This can hinder identification of significant source correlation and self-consistency since simultaneous decreases in P_{KS} and P_{bin} may not be observed.

There are some of the limitations of the FSM. Specifically, all scenarios incorporating an iron composition are found to be consistent with isotropy. This is to be expected since the arrival directions of UHECR iron primaries have been effectively isotropized with respect to the hypothesized source distributions by the GMF for all but the smallest B_\odot ⁶. Magnetic parameter space would have to be so finely gridded to see meaningful variation in P_{KS} and P_{bin} as to be computationally limited.

SUMMARY

A method for determining the self-consistency of GMF and UHECR property hypothesis sets based on cosmic rays observations has been presented and validated using simple and realistic scenarios. Two complementary procedures are utilized which determine the correlation excess beyond the isotropic expectation as well as the behavior of the entirety of backtracked cosmic ray observations relative to that of the same isotropic simulations. The FSM finds regions of magnetic field parameter space within a given overall hypothesis set which are maximally inconsistent with an isotropic assumption. No false positives are found for the tested scenarios⁷. Thus, parameter space of a hypothesis set where an already existing anisotropy is neither maintained nor increased can be efficiently eliminated from consideration as theories describing the UHECR observations.

The FSM does have limitations. The method depends on finding regions of parameter

⁶ As stated above the FSM relies on the existence of an underlying anisotropy in the observed arrival directions of UHECRs.

⁷ Only regions near a truth scan point show a significant decrease in the consistency with isotropy.

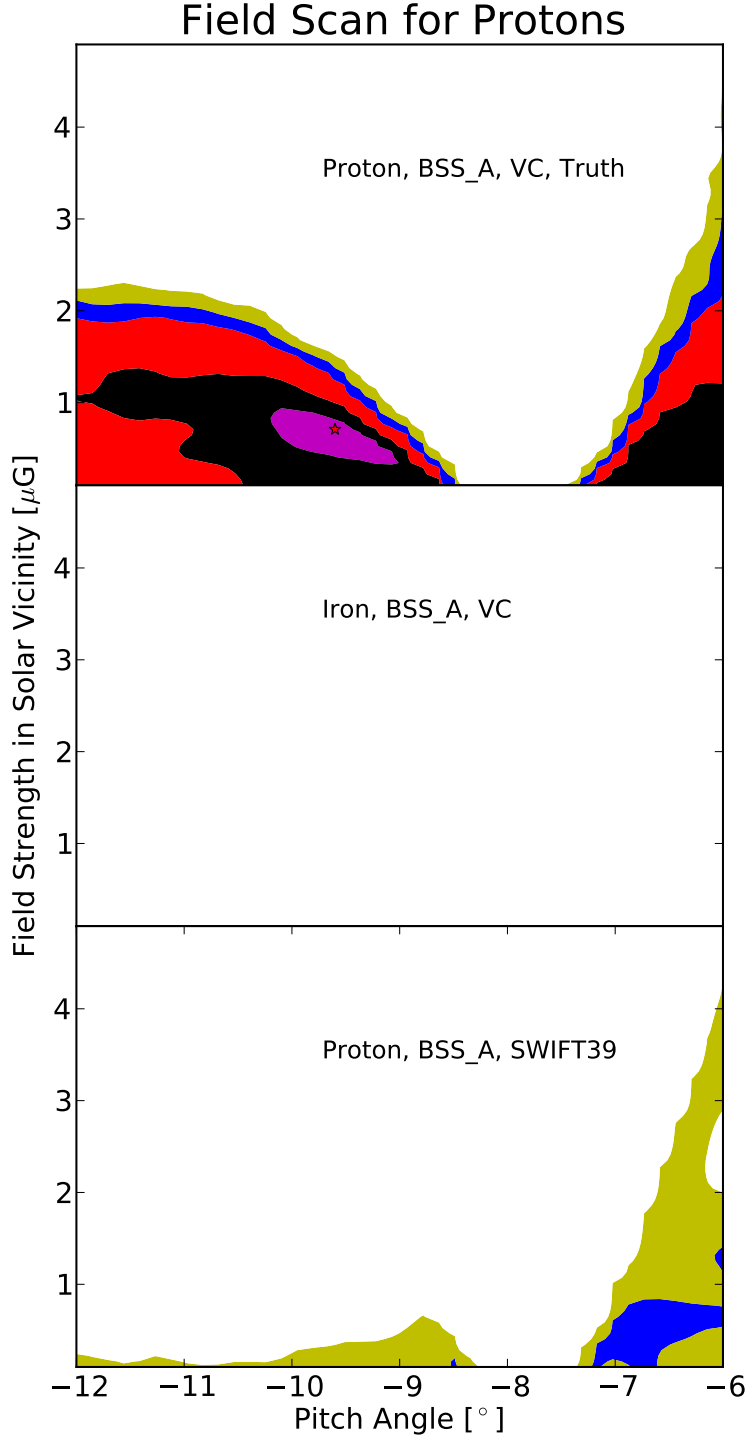


FIG. 12: Contour plot of P_{KS} for a realistic scenario. The subplots are labelled with their hypothesis set components. The color scale of P_{KS} is White, $P_{KS} \geq 10^{-4}$; Yellow, $10^{-4} > P_{KS} \geq 10^{-5}$; Blue, $10^{-5} > P_{KS} \geq 10^{-6}$; Red, $10^{-6} > P_{KS} \geq 10^{-8}$; Black, $10^{-8} > P_{KS} \geq 10^{-10}$; Magenta, $10^{-10} > P_{KS}$. The star in the top subplot indicates the truth hypothesis set parameters.

space where anisotropic observations remain inconsistent with isotropic observations even after backtracking. As such the method cannot be used on UHECR observations without an already existing observed anisotropy or with a composition hypothesis dominated by high Z UHECR.

* Author's email: msutherland@phys.lsu.edu

† Author's email: bbaugh@mps.ohio-state.edu

‡ Department of Physics and the Center for Cosmology and Astro-Particle Physics, The Ohio State University, Columbus, Ohio 43210, USA

§ Author's email: beatty@mps.ohio-state.edu

- [1] The Pierre Auger Collaboration, *Science* **318**, 938 (Nov. 2007), arXiv:0711.2256
- [2] The Pierre Auger Collaboration, *Astroparticle Physics* **31**, 399 (Jul. 2009), arXiv:0903.1127 [astro-ph.HE]
- [3] P. P. Kronberg, *Reports on Progress in Physics* **57**, 325 (Apr. 1994)
- [4] P. P. Kronberg, in *Workshop on Observing Giant Cosmic Ray Air Showers From $\dot{10}(20)$ eV Particles From Space*, American Institute of Physics Conference Series, Vol. 433, edited by J. F. Krizmanic, J. F. Ormes, & R. E. Streitmatter (1998) pp. 196–211
- [5] R. Beck, *Space Sci. Rev.* **99**, 243 (Oct. 2001), arXiv:astro-ph/0012402
- [6] P. P. Kronberg, *Astronomische Nachrichten* **327**, 517 (Jun. 2006)
- [7] R. Beck, in *American Institute of Physics Conference Series*, American Institute of Physics Conference Series, Vol. 1085, edited by F. A. Aharonian, W. Hofmann, & F. Rieger (2008) pp. 83–96, arXiv:0810.2923
- [8] D. Ryu, H. Kang, and P. L. Biermann, *A&A* **335**, 19 (Jul. 1998), arXiv:astro-ph/9803275
- [9] G. Sigl, F. Miniati, and T. A. Enßlin, *Phys. Rev. D* **70**, 043007 (Aug. 2004), arXiv:astro-ph/0401084
- [10] K. Dolag, D. Grasso, V. Springel, and I. Tkachev, *Soviet Journal of Experimental and Theoretical Physics Letters* **79**, 583 (2004), arXiv:astro-ph/0310902
- [11] K. Dolag, D. Grasso, V. Springel, and I. Tkachev, *J. Cosmology Astropart. Phys.* **1**, 9 (Jan. 2005), arXiv:astro-ph/0410419
- [12] S. Das, H. Kang, D. Ryu, and J. Cho, *Journal of Physics Conference Series* **120**, 062025 (Jul.

- 2008), arXiv:0706.2597
- [13] D. Ryu, S. Das, and H. Kang, ApJ **710**, 1422 (Feb. 2010), arXiv:0910.3361 [astro-ph.HE]
 - [14] T. Stanev, ApJ **479**, 290 (Apr. 1997), arXiv:astro-ph/9607086
 - [15] G. A. Medina Tanco, E. M. de Gouveia dal Pino, and J. E. Horvath, ApJ **492**, 200 (Jan. 1998), arXiv:astro-ph/9707041
 - [16] D. Harari, S. Mollerach, and E. Roulet, Journal of High Energy Physics **8**, 22 (Aug. 1999), arXiv:astro-ph/9906309
 - [17] D. Harari, S. Mollerach, and E. Roulet, Journal of High Energy Physics **2**, 35 (Feb. 2000), arXiv:astro-ph/0001084
 - [18] H. Takami, H. Yoshiguchi, and K. Sato, ApJ **639**, 803 (Mar. 2006), arXiv:astro-ph/0506203
 - [19] M. Kachelrieß, P. D. Serpico, and M. Teshima, Astroparticle Physics **26**, 378 (Jan. 2007), arXiv:astro-ph/0510444
 - [20] H. Takami and K. Sato, ApJ **681**, 1279 (Jul. 2008), arXiv:0711.2386
 - [21] D. S. Mathewson and V. L. Ford, MmRAS **74**, 139 (1970)
 - [22] C. Heiles, ApJ **462**, 316 (May 1996)
 - [23] C. Heiles, AJ **119**, 923 (Feb. 2000), arXiv:astro-ph/9910303
 - [24] R. J. Rand and A. G. Lyne, MNRAS **268**, 497 (May 1994)
 - [25] J. L. Han, R. N. Manchester, A. G. Lyne, and G. J. Qiao, ApJ **570**, L17 (May 2002), arXiv:astro-ph/0203517
 - [26] R. Beck, Ap&SS **289**, 293 (Feb. 2004), arXiv:astro-ph/0310287
 - [27] J. C. Brown, M. Haverkorn, B. M. Gaensler, A. R. Taylor, N. S. Bizunok, N. M. McClure-Griffiths, J. M. Dickey, and A. J. Green, ApJ **663**, 258 (Jul. 2007), arXiv:0704.0458
 - [28] M. Opher, F. A. Bibi, G. Toth, J. D. Richardson, V. V. Izmodenov, and T. I. Gombosi, Nature **462**, 1036 (Dec. 2009)
 - [29] E. M. Berkhuijsen, A&A **14**, 359 (Oct. 1971)
 - [30] W. N. Brouw and T. A. T. Spoelstra, A&AS **26**, 129 (Oct. 1976)
 - [31] C. Heiles, in *Polarimetry of the Interstellar Medium*, Astronomical Society of the Pacific Conference Series, Vol. 97, edited by W. G. Roberge & D. C. B. Whittet (1996) pp. 457–+
 - [32] S. A. Mao, B. M. Gaensler, M. Haverkorn, E. G. Zweibel, G. J. Madsen, N. M. McClure-Griffiths, A. Shukurov, and P. P. Kronberg, ApJ **714**, 1170 (May 2010), arXiv:1003.4519 [astro-ph.GA]

- [33] R. M. Crocker, D. I. Jones, F. Melia, J. Ott, and R. J. Protheroe, *Nature* **463**, 65 (Jan. 2010), arXiv:1001.1275 [astro-ph.GA]
- [34] A. Berdyugin and P. Teerikorpi, *A&A* **368**, 635 (Mar. 2001)
- [35] X.-H. Sun and W. Reich, *Research in Astronomy and Astrophysics* **10**, 1287 (Dec. 2010), arXiv:1010.4394 [astro-ph.GA]
- [36] J. L. Han, R. N. Manchester, A. G. Lyne, G. J. Qiao, and W. van Straten, *ApJ* **642**, 868 (May 2006), arXiv:astro-ph/0601357
- [37] C. L. Van Eck, J. C. Brown, J. M. Stil, K. Rae, S. A. Mao, B. M. Gaensler, A. Shukurov, A. R. Taylor, M. Haverkorn, P. P. Kronberg, and N. M. McClure-Griffiths, *ApJ* **728**, 97 (Feb. 2011), arXiv:1012.2938 [astro-ph.GA]
- [38] H. Men, K. Ferrière, and J. L. Han, *A&A* **486**, 819 (Aug. 2008), arXiv:0805.3454
- [39] R. Jansson, G. R. Farrar, A. H. Waelkens, and T. A. Enßlin, *J. Cosmology Astropart. Phys.* **7**, 21 (Jul. 2009), arXiv:0905.2228 [astro-ph.GA]
- [40] J. P. Vallée, *New A Rev.* **48**, 763 (Sep. 2004)
- [41] D. Elstner, K. Otmianowska-Mazur, S. von Linden, and M. Urbanik, *A&A* **357**, 129 (May 2000)
- [42] X. H. Sun, W. Reich, A. Waelkens, and T. A. Enßlin, *A&A* **477**, 573 (Jan. 2008), arXiv:0711.1572
- [43] F. S. Tabatabaei, M. Krause, A. Fletcher, and R. Beck, *A&A* **490**, 1005 (Nov. 2008), arXiv:0809.0419
- [44] R. Beck, *Ap&SS* **320**, 77 (Apr. 2009), arXiv:0711.4700
- [45] U. Klein, R. Wielebinski, and H. W. Morsi, *A&A* **190**, 41 (Jan. 1988)
- [46] K. T. Chyży and R. Beck, *A&A* **417**, 541 (Apr. 2004), arXiv:astro-ph/0401157
- [47] R. Beck, A. Fletcher, A. Shukurov, A. Snodin, D. D. Sokoloff, M. Ehle, D. Moss, and V. Shoutenkov, *A&A* **444**, 739 (Dec. 2005), arXiv:astro-ph/0508485
- [48] A. M. Wolfe, R. A. Jorgenson, T. Robishaw, C. Heiles, and J. X. Prochaska, *Nature* **455**, 638 (Oct. 2008), arXiv:0811.2408
- [49] P. G. Tinyakov and I. I. Tkachev, *Astroparticle Physics* **18**, 165 (Oct. 2002), arXiv:astro-ph/0111305
- [50] M. S. Sutherland, *A Method for Establishing Constraints on Galactic Magnetic Field Models Using Ultra High Energy Cosmic Rays and Results from the Data of the Pierre Auger Ob-*

- servatory*, PhD dissertation, The Ohio State University, Department of Physics (Jun. 2010), http://etd.ohiolink.edu/view.cgi?acc_num=osu1274798328
- [51] The Pierre Auger Collaboration: J. Abraham, P. Abreu, M. Aglietta, C. Aguirre, E. J. Ahn, D. Allard, I. Allekotte, J. Allen, J. Alvarez-Muñiz, M. Ambrosio, and et al., ArXiv e-prints(Jun. 2009), arXiv:0906.2347 [astro-ph.HE]
 - [52] E. Roulet, International Journal of Modern Physics A **19**, 1133 (2004), arXiv:astro-ph/0310367
 - [53] M. Sutherland, B. Baughman, and J. Beatty, Astroparticle Physics **34**, 198 (2010), ISSN 0927-6505, <http://www.sciencedirect.com/science/article/B6TJ1-50N2P6R-1/2/8246f10a9b1bceb069ef052a0be233c4>
 - [54] P. L. Biermann, J. K. Becker, L. Caramete, A. Curuțiu, R. Engel, H. Falcke, L. Á. Gergely, P. G. Isar, I. C. Mariș, A. Meli, K. Kampert, T. Stanev, O. Tașcău, and C. Zier, Nuclear Physics B Proceedings Supplements **190**, 61 (May 2009), arXiv:0811.1848
 - [55] G. Cusumano, V. La Parola, A. Segreto, V. Mangano, C. Ferrigno, A. Maselli, P. Romano, T. Mineo, B. Sbarufatti, S. Campana, G. Chincarini, P. Giommi, N. Masetti, A. Moretti, and G. Tagliaferri, A&A **510**, A48+ (Feb. 2010), arXiv:0906.4788 [astro-ph.HE]
 - [56] M. Prouza and R. Šmída, A&A **410**, 1 (Oct. 2003), arXiv:astro-ph/0307165
 - [57] M. Veron-Cetty and P. Veron, VizieR Online Data Catalog **7248**, 0 (Jun. 2006)
 - [58] The Pierre Auger Collaboration, C. Bonifazi, and the Pierre Auger Collaboration, Nuclear Physics B Proceedings Supplements **190**, 20 (May 2009)